

# Observation of tunable charged exciton polaritons in hybrid monolayer $\text{WS}_2$ – plasmonic nanoantenna system

Jorge Cuadra,<sup>1,\*</sup> Denis G. Baranov,<sup>1</sup> Martin Wersäll,<sup>1</sup>

Ruggero Verre,<sup>1</sup> Tomasz J. Antosiewicz,<sup>1,2</sup> and Timur Shegai<sup>1,†</sup>

<sup>1</sup>*Department of Physics, Chalmers University of Technology, 412 96, Göteborg, Sweden.*

<sup>2</sup>*Centre of New Technologies, University of Warsaw,  
Banacha 2c, 02-097 Warsaw, Poland.*

## Abstract

Formation of dressed light-matter states in optical structures, manifested as Rabi splitting of the eigen energies of a coupled system, is one of the key effects in quantum optics. In pursuing this regime with semiconductors, light is usually made to interact with excitons – electrically neutral quasiparticles of semiconductors, meanwhile interactions with charged three-particle states – trions – have received little attention. Here, we report on strong interaction between plasmons in silver nanoprisms and charged excitons – trions – in monolayer tungsten disulphide ( $\text{WS}_2$ ). We show that the plasmon-exciton interactions in this system can be efficiently tuned by controlling the charged versus neutral exciton contribution to the coupling process. In particular, we show that a stable trion state emerges and couples efficiently to the plasmon resonance at low temperature by forming three bright intermixed plasmon-exciton-trion polariton states. Our findings open up a possibility to exploit electrically charged trion polaritons – previously unexplored mixed states of light and matter in nanoscale hybrid plasmonic systems.

---

\* jorge.cuadra@chalmers.se

† timurs@chalmers.se

Interaction between light and matter is at the heart of modern optics. It is present in atomic physics as well as in solid state systems and plays an essential role in cavity quantum electrodynamics (cQED). A regime that attracts significant interest is achieved when the exchange of energy between photons and matter excitations becomes faster than the decoherence rates of both subsystems [1–4]. Under these conditions one observes the formation of polaritons that are hybrid states possessing both light and matter characteristics. Recently it has been shown that metallic nanoparticles enable this non-perturbative regime of light-matter interaction due to a combination of deeply subwavelength confinement of electromagnetic radiation with large transition dipole moments of molecular and quantum dot excitons [5–9].

Monolayers of transition metal dichalcogenides (TMDCs) are semiconductor materials with a direct band gap transition [10], where neutral ( $X^0$ ) and charged ( $X^{+/-}$ ) excitons (or trions) are stable and can be excited either by optical or electrical means [11–13]. The large spin-orbit coupling in these materials permits a spin-valley degree of freedom accessible by optical dichroism [14, 15]. In addition, the broken inversion symmetry puts the band gap at the edges of the Brillouin zone allowing valley-selective excitations by pumping with a circularly polarized light. The absorption of TMDCs monolayers is very high and can reach values of 3% for MoS<sub>2</sub> and as much as 10% for WS<sub>2</sub> at resonance [16].

The high absorptivity of TMDCs monolayers makes them ideal candidates for realization of the strong coupling regime. Indeed, observations of strong coupling between TMDCs and nanophotonic resonators have been reported in several different systems including optical microcavities [17–19] and diffractive modes of plasmonic nanoparticle arrays [20, 21]. At the single plasmonic nanoparticle level there is no clear evidence of reaching the strong coupling regime, although efforts have been made [22]. Additionally, a number of recent works report on photoluminescence (PL) modification and enhancement as a result of plasmon-exciton coupling in the weak coupling regime [23–27]. It is important to note that, molecular J-aggregates, which have been extensively used to achieve the strong coupling regime [5, 6, 9], [28, 29], suffer from optical bleaching and are not stable under ambient conditions. In contrast to that, monolayer TMDCs are chemically inert, stable and robust at ambient conditions, which makes them advantageous for active and nonlinear plasmonics applications.

One of the key features of hybrid plasmon-exciton systems is the possibility for active control and saturation. Such active control has been demonstrated in various hybrid nanos-

structures. Examples include controllable and reversible switching of the strong coupling regime in microcavities loaded with photochromic molecules [30] and for silver nanoparticle arrays via UV illumination [31]. Ultrafast tuning of strongly-coupled metal-molecular aggregates via femtosecond pumping has also been observed [32, 33]. Demonstration of thermalization, cooling and lasing of plasmon-exciton polaritons have been reported recently [34–36]. However, in these works reversible switching and active control was demonstrated in the systems that involved only electrically neutral excitations.

Conversely, little attention has been devoted to strong coupling with charged excitons. Such interactions would result in the formation of exciton polaritons carrying a non-zero net electrical charge. These phenomena have been previously observed in microcavities loaded with quantum wells [37–39], charged quantum dots [40] and more recently in tunable polaron polaritons [19]. The sole existence of these quasiparticles opens a number of intriguing perspectives, as such “charged” polaritons are anticipated to strongly interact with each other and to improve charge and exciton transport properties mediated by strong coupling [39, 41].

Here, we demonstrate strong interactions between plasmons in an individual silver nanoprism and neutral as well as charged excitons in monolayer  $\text{WS}_2$ . The latter is especially interesting, as this opens up a new way to control and manipulate charge via light-matter interactions. To the best of our knowledge this is the first demonstration of this kind using an individual plasmonic nanoantenna. In this study we show that the degree of plasmon-exciton-trion coupling can be tailored by temperature. In particular, by scanning the temperature in the range between 77 and 300 K, we are able to observe a transition from two polaritonic resonances at room temperature, corresponding to plasmon-exciton interaction, to the formation of three polaritonic resonances at  $T=77$  K, corresponding to both exciton and trion strongly coupled to the plasmonic cavity.

## RESULTS

**System under study.** The coupled system in this work is composed of colloidal silver nanoprisms positioned on top of a monolayer  $\text{WS}_2$ . We start by preparing the monolayer structure by mechanical exfoliation from a high quality crystal and transferring it to a thermally oxidized silicon substrate. Note that the monolayer flake size can readily reach sizes greater than  $\sim 100$  micrometers (see Fig. 1a) The monolayer nature of the  $\text{WS}_2$  flake is

confirmed by optical contrast and the bright PL signal – typical for direct bandgap semiconductors (Fig. 1b). The PL spectrum at 300 K under ambient conditions has the resonance at 2.012 eV ( $\omega_{X^0}$ ) and corresponds to the neutral A-exciton with a binding energy of about 700 meV [42]. The PL signal at 77 K, in contrast to the room temperature data exhibits two peaks: the high-energy resonance (2.07 eV) and the low-energy peak (2.03 eV) (blue curve in Fig. 1b). We assign the former to the neutral A-exciton, which undergoes a blue-shift, whereas the latter corresponds to the positively charged exciton ( $\omega_{X^+}$ ) – i.e. a trion. The trion state dominates the PL at low T and has a binding (or dissociation) energy of about 40 meV in agreement with earlier reports [42]. The trion state is likely positively charged  $-\omega_{X^+}$  because of the positively charged polymer adhesion layer used in this study to bind plasmonic nanostructures (see Methods and Supplementary Information (SI)).

The second ingredient to construct the hybrid system in this study is the silver nanoprism (see Fig. 1d). These nanoparticles were prepared by a seed mediated colloidal synthesis and are single crystalline in nature, which greatly improves the quality factor of the plasmon resonance and thus the accessibility of the strong coupling [43]. A typical nanoprism has dimensions of about 60-80 nm in side length and about 10 nm in thickness. Such nanoprism dimensions result in a plasmon resonance,  $\omega_{pl}$ , overlapping with the exciton transition,  $\omega_{X^0}$ , in the monolayer WS<sub>2</sub> in the coupled system. Thus by combining these two materials one could expect strong plasmon-exciton interactions. In order to verify this expectation, we positioned Ag nanoprisms on top of the monolayer by drop casting a nanoparticle suspension on a polymer pre-coated substrate (see Methods). As a result we obtain a WS<sub>2</sub> flake covered with Ag nanoprisms of various sizes as is evidenced by the dark-field (DF) optical microscopy (see Fig. 1c). The colourful spots in the image are individual Ag nanoprisms possessing different plasmon resonances. This allows us to study a variety of plasmon-exciton resonance detunings  $\delta = \omega_{pl} - \omega_{X^0}$  within the same sample. A combined 2D material - silver nanoprism system is depicted schematically in Fig. 1d. The optical states are localized at the corners of the prism and are shown schematically by the bright spots. Insets show a magnified DF image of a single nanoprism and an SEM image of the coupled system. The latter confirms that an individual nanoprism is measured in the optical microscope.

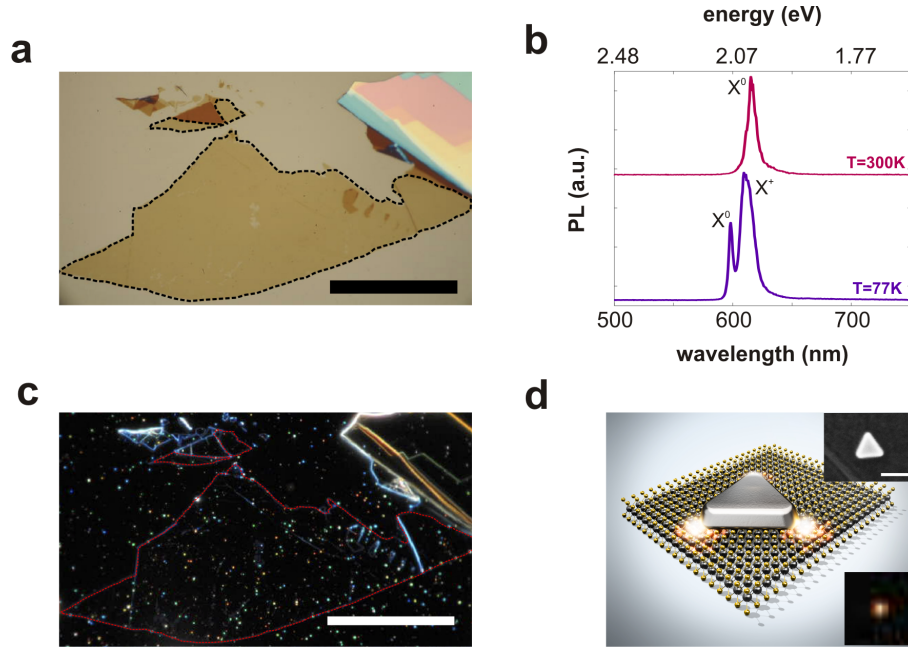


Figure 1. **Hybrid 2D material – nanoparticle plasmon system.** (a) Bright field optical image of the exfoliated  $\text{WS}_2$  flake. Monolayer regions are marked by the dotted line (scale bar  $50 \mu\text{m}$ ) (b) PL spectra of the  $\text{WS}_2$ . The red curve shows the PL taken at ambient conditions, the resonance, at  $616 \text{ nm}$ , corresponds to the neutral A-exciton. The blue curve depicts the PL at  $77 \text{ K}$ , the peak at  $598 \text{ nm}$  is the neutral A-exciton that has blue-shifted. The peak at  $611 \text{ nm}$  is a charged exciton and dominates the PL emission. (c) DF microscope image of the  $\text{WS}_2$  flake covered with silver nanoprisms. Monolayer regions are marked by the dotted line (scale bar  $50 \mu\text{m}$ ). (d) Artist view of the hybrid system: high density of photonic states (hot-spots) is shown at the corners of the nanoprism, which overlaps with the  $\text{WS}_2$  monolayer for efficient plasmon-exciton interaction. Inset shows the SEM image of such particle (scale bar  $100 \text{ nm}$ ) and a magnified view of the DF image.

**Temperature dependence.** We now explore the evolution of the strongly coupled system by varying its temperature (see Methods for experimental details). Since the PL spectrum exhibits the appearance of a trion resonance at low temperature, one could expect strong interaction between the trion and the plasmon. The DF spectrum of the hybrid system (Fig. 2) measured at ambient conditions reveals the splitting of the resonance into two peaks, which demonstrates the formation of plasmon-exciton polaritons. The high-energy peak represents the upper polariton and the low-energy peak is the lower polariton. The dip between the polaritonic branches coincides with  $\omega_{X^0}$ . Upon decreasing the temperature

down to liquid nitrogen (77 K), the charged state of the exciton is clearly observed and starts dominating the PL spectrum (see Fig. 1b and SI Fig. S3). As this resonance is split from the exciton by only  $\sim 40$  meV, the strong interaction of both exciton and trion resonances with the plasmonic cavity is plausible. This is revealed by the appearance of two dips in the DF spectrum that match the energies of the exciton and trion states (see Fig. 2 T=77 K).

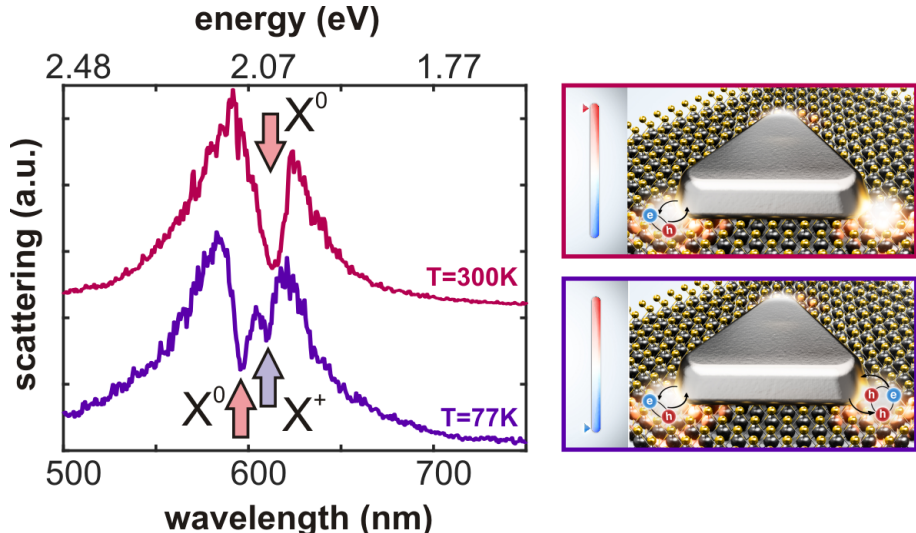


Figure 2. **Coupled system under room and liquid nitrogen temperature.** Left: Dark-field scattering spectra at 77 and 300 K. At ambient conditions the DF spectrum depicts two peaks, namely the upper and lower polaritons. At liquid nitrogen temperature the DF spectrum shows three peaks that are identified as upper middle and lower polaritons. Arrows show neutral ( $X^0$ ) and charged ( $X^+$ ) exciton resonance wavelengths. Right: Artist view of plasmon-exciton mixture at T=300 K and plasmon-exciton-trion interaction at T=77 K.

The hybrid system thus experiences a transition from plasmon-exciton interaction at room temperature to a more complex plasmon-exciton-trion interaction at low temperature, which is schematically illustrated in Fig. 2 (right panel). This evolution was studied by measuring the DF scattering as a function of temperature. The results for the hybrid system with approximately zero detuning (the detuning is defined at 77 K) are presented in Fig. 3a. The cases of positive and negative detuning are shown in the SI (Fig. S2). Irrespectively of the detuning, however, the temperature induced modifications are similar: two dips are clearly observed at low temperature, which demonstrate that both the neutral exciton (the high-energy dip) and the trion (the low-energy dip) interact strongly with the plasmonic

cavity.

The coupled plasmon-exciton-trion system thus results in a formation of three bright hybrid states – upper, middle and lower polaritons. The corresponding exciton, trion and plasmon contributions can in principle be inferred from the spectral data. Notably, all polaritons possess non-vanishing contributions of all three system subparts – excitonic, trionic and plasmonic. For this reason these states are potentially interesting for charge transport as they carry non-zero net electrical charge (positive in this case). The composition of these states can be understood by diagonalizing the  $3 \times 3$  Hamiltonian of the system [37]:

$$\begin{pmatrix} \omega_{pl} - i\gamma_{pl} & g_{X^0} & g_{X^+} \\ g_{X^0} & \omega_{X^0} - i\gamma_{X^0} & 0 \\ g_{X^+} & 0 & \omega_{X^+} - i\gamma_{X^+} \end{pmatrix} \quad (1)$$

with  $g_{X^0}$  and  $g_{X^+}$  being the interaction constants of plasmon with exciton and trion, respectively and  $\gamma_{X^0}$  ( $\gamma_{X^+}$ ) corresponds to the dissipation rate of the exciton (trion). The main conclusion of this analysis is that for the appropriate parameters there exists a solution with three bright polariton states. The middle polariton has a relatively small,  $\sim 20\%$ , plasmon component (which vanishes completely in the very strong coupling regime), while both upper and lower polaritons are composed roughly of  $\sim 50\%$  plasmon and of  $\sim 25\%$  exciton and  $\sim 25\%$  trion respectively (see SI, Fig. S7).

As the temperature rises, the dip associated with the trion state becomes less pronounced and completely disappears at 300 K. Such behavior is consistent with the PL measurements and reflectivity data of the bare monolayer  $\text{WS}_2$  (see SI Fig. S3) and can be explained by taking into account the loss of oscillator strength by the trion as the temperature is increased [44]. Additionally, note that the binding (dissociation) energy of the trion is about 40 meV, which is comparable to  $k_B T$  at room temperature thus making the trion less stable at elevated temperatures.

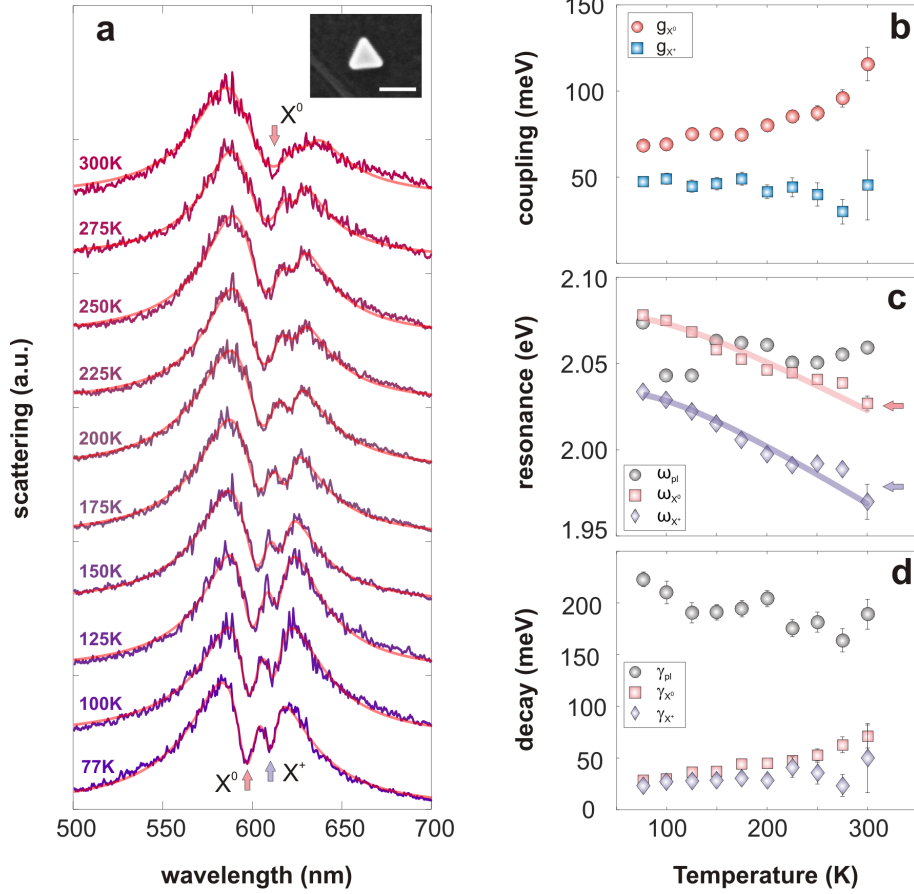


Figure 3. **Temperature dependence of the coupled system.** (a) Dark field spectra for an individual silver nanoprism – monolayer  $WS_2$  hybrid as a function of temperature. Semi-transparent red curves show coupled oscillator model fits of the data. Inset: SEM image of the corresponding nanostructure (scale bar - 100 nm). (b-d) Temperature dependence of the coupled oscillator model parameters. (b) Coupling rates for exciton and trion, (c) resonance energies of plasmon, exciton and trion resonances. Solid lines show a fit using the semiconductor model. The O’Donnell model gives the following values of  $E_g(0) = 2.08$  eV (2.03 eV),  $S = 1.82$  (2.17) and  $\langle \hbar\omega \rangle = 26$  meV (26 meV) for  $X^0$  ( $X^+$ ) correspondingly for the coupled case. (d) Decay rates for plasmon, exciton and trion correspondingly.

The strong interaction between the plasmon and neutral exciton, however, remains throughout the whole temperature range studied. This is likely due to the fact that the exciton increases its oscillator strength as the temperature rises. It is also important to note that the binding energy of the exciton, which is on the order of  $\sim 700$  meV, is much above the thermal energy and thus thermal dissociation and broadening does not prevent the coupling even at room temperature.

The temperature dependence of the oscillator strength can be understood by noting that the oscillator strength depends on the number of available states. By decreasing the temperature the distribution of states changes in favour of trions. Thus the trions gain and the neutral excitons lose the oscillator strength upon cooling [44]. This is consistent with our observations.

**Coupled oscillator model.** We now turn to an in-depth analysis of the temperature scans. We use a modified coupled harmonic oscillator model to extract the parameters of the hybrid system. This model considers a cavity driven by an external field, which is coupled to two dissipative oscillators [45, 46] (see Methods). In this case, we consider coupling to neutral and charged excitons. The scattering cross-section of such a system is then given by:

$$\sigma_{scat} \propto \left| \frac{\omega^2 \tilde{\omega}_{X0}^2 \tilde{\omega}_{X+}^2}{\tilde{\omega}_{X0}^2 \tilde{\omega}_{pl}^2 \tilde{\omega}_{X+}^2 - \omega^2 (g_{X0}^2 \tilde{\omega}_{X+}^2 + g_{X+}^2 \tilde{\omega}_{X0}^2)} \right|^2 \quad (2)$$

with

$$\begin{aligned} \tilde{\omega}_{X0}^2 &= (\omega^2 - \omega_{X0}^2 + i\gamma_{X0}\omega), \\ \tilde{\omega}_{X+}^2 &= (\omega^2 - \omega_{X+}^2 + i\gamma_{X+}\omega), \\ \tilde{\omega}_{pl}^2 &= (\omega^2 - \omega_{pl}^2 + i\gamma_{pl}\omega) \end{aligned}$$

being the harmonic oscillator terms for the exciton, trion and plasmon, respectively.

We further utilize Eq. (2) to fit the temperature-dependent DF scattering spectra. We observe that the coupled oscillator model reproduces the experimental results exceptionally well (see semi-transparent red curves in Fig. 3a). The parameters extracted from the coupled oscillator model as a function of temperature are shown in Fig. 3b-d.

The first important observation is that the coupling to the neutral excitons  $g_{X0}$  drops, whereas the coupling to the trions  $g_{X+}$  increases upon cooling (Fig. 3b). This ultimately leads to the emergence of the two dips in the scattering spectra at low temperature. At the same time at high temperature, coupling to trions essentially vanishes. This is confirmed by a substantial degradation of the fit quality for T=300 K (note the error bars for the trion coupling rate at T=300 K). This is in agreement with the qualitative analysis above, where we argued that the trion becomes less stable at room temperature. Notably, at room temperature the interaction becomes rather weak and Fano-like despite the relatively high

value of the coupling strength with respect to decoherence rates of the plasmon and the exciton. This is because of the large plasmon-exciton detuning at room temperature (see Fig. 3a,c T=300 K).

Another important observation is that both the trion and the exciton resonances blue-shift upon cooling (Fig. 3c). This is in agreement with the standard semiconductor behavior [47] and is confirmed here on the bare monolayer WS<sub>2</sub> (see SI Fig. S3 and S5). The fact that the exciton and trion resonances follow the temperature dependence that is consistent with the standard semiconductor behavior even in the coupled system signals that the coupled oscillator model provides a meaningful physical picture and therefore justifies its use. Indeed, temperature dependence of the semiconductor bandgap is conveniently described by the O'Donnell model for the temperature dependency of the semiconductor energy gap [47],

$$E_g(T) = E_g(0) - S \langle \hbar\omega \rangle \{ \coth [\langle \hbar\omega \rangle / 2k_B T] - 1 \} \quad (3)$$

where  $E_g(0)$  is the bandgap at 0 K,  $S$  is the electron-phonon coupling strength, and  $\langle \hbar\omega \rangle$  is the average phonon energy. This model fits our data both coupled (Fig. 3c) and uncoupled (see SI, Fig. S5) very well. The obtained values are consistent with earlier studies [12], which again justifies the use of the coupled oscillator model. Furthermore, we observe that the dissociation energy,  $\omega_{X^0} - \omega_{X^+}$ , is nearly constant in the studied temperature range and is about 40 meV (see Fig. 3c and Fig. S3).

We note that for the uncoupled nanoparticle system the plasmon resonance is expected to red shift upon cooling [48] (see SI, Fig. S1). However, in the coupled system this behavior is not observed (see Fig. 3c). We argue that this is due to interaction with the TMDC material, which “pulls” the plasmon resonance to higher energies at low temperature. In other words, exciton and trion resonances follow the standard semiconductor temperature dependence in accordance with Eq. (2), while the plasmon passively follows the change in its immediate dielectric environment induced by temperature changes.

We further extract and compare the decoherence rates to elucidate on whether or not the strong coupling condition is met (see Figs. 3b,d). We note that the strict condition for the strong coupling regime, that is,  $2g_{X^0} > \gamma_{pl}$ , is satisfied for neutral excitons but not for trions ( $2g_{X^+} > \gamma_{pl}$ ) at high temperature. As we show in the SI this regime manifests itself through several observable Rabi cycles (see Fig. S6). At high temperatures the trion is in the weak coupling regime as the coupling becomes less than both cavity and trion

dissipation rates  $2g_{X^+} < \gamma_{pl}, \gamma_{X^+}$  [18]. At high temperatures, however, the system is in the intermediate regime for the independent exciton and trion contributions –  $\gamma_{pl} > 2g_{X^0} > \gamma_{X^0}$  (or  $\gamma_{pl} > 2g_{X^+} > \gamma_{X^+}$ ) [46, 49], while the combined coupling still exceeds the strong coupling limit, i.e.  $2\sqrt{g_{X^0}^2 + g_{X^+}^2} \gtrsim \gamma_{pl}$ . We thus conclude that the combined plasmon-exciton-trion system reaches the strong coupling regime. Noteworthy, the plasmon-trion coupling here,  $g_{X^+} \approx 50$  meV, exceeds the trion binding energy,  $\omega_{X^0} - \omega_{X^+} \approx 40$  meV, which is an interesting regime since the light-matter coupling surpasses the Coulomb interaction in this case. It was recently predicted that in this regime the trion orbital and spin properties are strongly modified [50]. In the following discussion, we calculate the scattering and absorption cross-sections of the coupled system to demonstrate this point more rigorously (Fig. 4).

In further analysis (Fig. 3d), we notice that the linewidth of excitons and trions reduces upon cooling, thus making the corresponding scattering dips more pronounced. Exciton line narrowing upon cooling is a well-documented behavior consistent with previous results [51, 52] and confirmed here for the uncoupled exciton and trion system (see SI, Fig. S3). At the same time plasmons in the coupled system do not narrow upon cooling (Fig. 3d). This is somewhat surprising considering that uncoupled plasmons are anticipated to red shift and slightly narrow upon cooling as was reported previously [48] and confirmed here in a control experiment (see SI Fig. S1). Such behavior is likely caused by the weak interaction with the TMDC material. Indeed both plasmon resonance and its full width half maximum depend on the electromagnetic environment, which is temperature-dependent in this case.

In closing the analysis section, we note that Fig. 3 corresponds to the case of zero detuning. Similar data is presented in the SI for the case of positive and negative detuning (see Fig. S2). These observations are reproducible and consistent with the coupled oscillator model. The data shows increase of trion coupling while reduction of exciton coupling upon cooling. At the same time, both the exciton and trion resonances narrow upon cooling. The data shows consistent blue shift in the exciton and the trion resonance upon cooling in agreement with the standard semiconductor behavior. Most notably, however, the data demonstrates reproducible coupling to the charged exciton at low temperature. This latter fact makes us confident to conclude we observe formation of charged polaritons in this system.

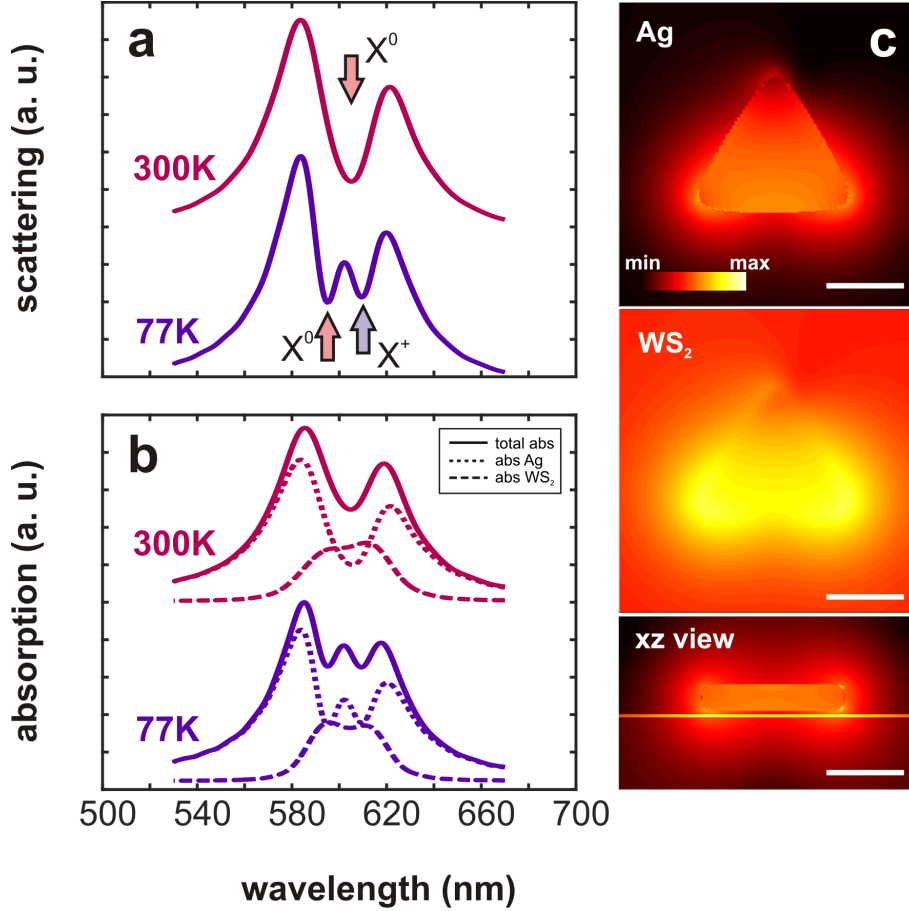


Figure 4. **Numerical simulation.** (a) Scattering cross-sections spectra as a function of temperature. At  $T=300$  K the dielectric function of  $WS_2$  was assumed to have only one resonance energy corresponding to uncharged exciton  $X^0$ , while at  $T=77$  K both  $X^+$  and  $X^0$  contribute to the signal. Parameters of the model:  $\epsilon_{Ag}(\omega)$  dielectric function for silver is taken from Palik [53],  $WS_2$  from Ref. [16], nanoprism side length  $L=70$  nm, height  $H=10$  nm, nanoprism edges are rounded with radius of curvature  $r \sim 5$  nm. TMDC layer was positioned on a dielectric slab with refracting index  $n = 1.5$  that mimics a glass substrate. The whole system is embedded in vacuum. (b) Total, silver and  $WS_2$  absorption cross-sections spectra as a function of temperature. Note splitting observed at both temperatures, which confirms the intermediate coupling regime. (c) Electromagnetic energy density distribution,  $\rho(r)$ , within the nanoparticle and the 2D material at  $\lambda = 577$  nm. Both top and side views are shown. Scale bar = 30 nm.

**Numerical calculations.** To gain further insight into the nature of plasmon-exciton-trion interactions in this system, we perform numerical calculations using the finite-difference time domain (FDTD) method (see Methods). The results reproduce all essential features

of the experiment and the analytical coupled oscillator model (see Fig. 4). This implies that, despite significant simplifications used in the coupled oscillator model, it adequately describes the data, even in a rather complex regime of two types of excitons involved in the coupling process such as studied here. We thus emphasize the power of the coupled oscillator model in describing such system.

Comparison between experimental observations and the FDTD calculations allows to estimate the oscillator strength corresponding to both neutral and charged excitons as well as to compare them to the values obtained from reflectivity and photoluminescence (see Fig. S3). The dielectric susceptibility of WS<sub>2</sub> monolayer at room temperature (corresponding solely due to neutral exciton contribution) was extracted from the literature values and was used here without any further open parameters [16]. The agreement between the FDTD calculations and experimental observations in Figs. 2-4 is striking. The low temperature  $\varepsilon(\omega)$  of WS<sub>2</sub> was introduced phenomenologically (by two Lorentzian contributions), yet it also leads to a good agreement between the experiment and the theory. Thus the phenomenological  $\varepsilon(\omega)$  at low temperature corresponds to the coupling rates of both neutral and charged excitons extracted from the coupled oscillator model (Fig. 3b).

In addition to the calculated scattering spectra (Fig. 4a), we perform calculations of absorption cross-section of the coupled system as well as its components – Ag nanoprism and WS<sub>2</sub> monolayer (Fig. 4b). The plots in Fig. 4b clearly show splitting of absorption in the Ag nanoprism, as well as smaller but visible splitting in the absorption spectra of the WS<sub>2</sub> monolayer. This is a signature of strong coupling [49]. The small splitting in the 2D material absorption is explained by a lack of long-lived oscillations between Ag and WS<sub>2</sub>. As shown in Fig. S6, the time evolution of the Rabi oscillations is short-lived and exhibits only one significant period. A similar observation can be drawn from the oscillations of the electric fields around the Ag triangle, where the excitation energy alternates between the plasmon-polariton (visible enhanced fields) and the 2D material (see SI movies).

We further inspect the electromagnetic energy density distributions,  $\rho(r)$ , [54] in the coupled system (Fig. 4c). We observe that the mode in the nanoprism is confined mainly to its interior. We also observe that while the energy density in the WS<sub>2</sub> is greater than in Ag, the monolayer occupies only a small volume due to its two-dimensionality and therefore the total energy stored in the metal and the 2D material is similar. For single nanoparticles the mode is concentrated within its volume [55–57] and to obtain long-lived Rabi oscillations

the excitonic material needs not only a large transition dipole moment, but also needs to saturate the small fraction of the mode present outside the metal resonator [6, 58]. In the present case this is not possible (Fig. 4c), yet filling up a small fraction of the mode volume with the 2D material is enough to reach the strong coupling. This is likely due to the large transition dipole moment of WS<sub>2</sub> ( $\mu_e = 56$  Debye [59]). We thus conclude that a coupled plasmon-exciton polariton system comprising a silver nanoprism and monolayer WS<sub>2</sub> is very useful for practical realization of strong coupling. One may ask how many excitons contribute to the coupling process in this case, especially taking in mind the large transition dipole moment of WS<sub>2</sub>. Following the well-known relation for the coupling strength  $g = \sqrt{N}\mu_e|E_{vac}| = \sqrt{N}\mu_e\sqrt{\hbar\omega/(2\varepsilon\varepsilon_0V)}$  and our previous estimations using J-aggregates [6], we obtain  $N \sim 10 - 20$  for realistic mode volumes in the range of  $V = (2 - 4) \times 10^4 \text{ nm}^3$ . This number closely approaches the quantum optics limit thus making this system potentially interesting for photon-photon interactions.

## DISCUSSION

To conclude, we have demonstrated that the optical response of the strongly coupled system can be tailored by tuning the temperature. At low temperatures the plasmonic cavity strongly interacts with both neutral and charged excitons in the monolayer WS<sub>2</sub>, whereas at room temperature only the neutral exciton is coupled to the plasmon. The hybrid structure in this study consists of an individual silver nanoprism and two-dimensional monolayer WS<sub>2</sub>. This system is extremely compact, yet able to strongly interact with light.

We note that the temperature-dependent PL signal of the WS<sub>2</sub> monolayer and in particular the second resonance at low energy appearing upon decreasing of temperature follows the trend associated with the trion state [12]. Other low energy states like bound states or localized excitons [60, 61] have lower dissociation energies and are not stable at elevated temperatures [62]. Based on this, we conclude that the low energy peak observed in the PL spectrum (Fig. 1b) and the low energy dip in the scattering spectra (Figs. 2-3) indeed appear due to the positively charged exciton – i.e. the trion. Here, the trion state is stabilized by low temperature and chemical doping [63].

Our findings demonstrate the principal possibility of studying electrically charged polaritons in a form of plasmon-exciton-trion hybrids. Here, this is done at low temperature to ensure the stability of the charged exciton state, however, by stabilization of the trion state

by other means, for example by electrostatic doping, similar effects can be anticipated at room temperature [42]. Constructing macroscopic coherent polariton states that will constitute a coherent mixture of excitons, trions and cavity excitations may find use in charge transport and optoelectronic devices by boosting the carrier mobility [41] in analogous way to the theoretically predicted exciton transport enhancement mediated by a cavity [64, 65]. This new degree of freedom – charged polaritons is the central observation of this work. We envision that these findings may find potential implications for various optoelectronic applications, such as light harvesting and light emitting devices.

## METHODS

**Sample preparation:** Silver nanoprisms were synthesized using a seed-mediated protocol [43].  $\text{WS}_2$  were mechanically exfoliated from bulk crystal (HQ-graphene) and transferred to a Si wafer with a thermally oxide layer (50 nm-thick) using the all-dry transfer method [66]. Monolayers were identified by photoluminescence spectra and optical contrast. In order to ensure a proper density of nanoprisms covering the monolayer flake, an adhesion layer was deposited before the nanoprism (Polylysine 0.25 mg/mL), then nanoparticles are drop-cast and let them rest for 2 min, the excess of solution is gently removed by an absorptive tissue. We note that the polymer layer that we utilize to adhere silver nanoprisms to the monolayer  $\text{WS}_2$  plays an important role in the stabilization of the trions. This is likely induced by the chemical doping [63]. The trion in this case is mostly a positively charged state since the adhesion layer tends to p-dope  $\text{WS}_2$ . To demonstrate this, in the SI (see Fig. S5) we perform a control experiment which shows that strong plasmon-trion coupling is not observed in the absence of the poly-lysine adhesion layer.

**Optical measurements:** Dark-field optical microscopy and spectroscopy measurements were done using a laser driven light source (ENERGETIQ EQ-99XFC) with side illumination configuration at an angle of about 50 degrees. For photoluminescence experiments, the sample was excited by a CW 532 nm (2.33 eV) laser under irradiance of  $\sim 100 \text{ W/cm}^2$ . PL and DF signals were collected using a  $20\times$  objective (Nikon, NA=0.45) and directed to a fibre-coupled 30 cm spectrometer (Andor Shamrock SR-303i) equipped with a CCD detector (Andor iDus 420). Low temperature measurements were performed using a cold finger optical cryostat (Janis).

**Coupled oscillators model:** Each component (plasmonic nanoparticle, exciton, and

trion) of the coupled system is described as a harmonic oscillator with its own resonance frequency and damping. Coupling between the nanoparticle and WS<sub>2</sub> excitations is mediated via inductive terms proportional to the oscillator velocities. Dynamics of the full system is therefore modeled by three coupled equations [45]:

$$\begin{aligned}\ddot{x}_{pl} + \gamma_{pl}\dot{x}_{pl} + \omega_{pl}^2 x_{pl} + g_{X^0}\dot{x}_{X^0} + g_{X^+}\dot{x}_{X^+} &= -eE(t) \\ \ddot{x}_{X^0} + \gamma_{X^0}\dot{x}_{X^0} + \omega_{X^0}^2 x_{X^0} - g_{X^0}\dot{x}_{pl} &= 0 \\ \ddot{x}_{X^+} + \gamma_{X^+}\dot{x}_{X^+} + \omega_{X^+}^2 x_{X^+} - g_{X^+}\dot{x}_{pl} &= 0\end{aligned}$$

Here,  $x_{pl}$ ,  $x_{X^0}$ , and  $x_{X^+}$  represent coordinates of the cavity, exciton, and trion oscillators, respectively,  $E(t)$  is the driving electric field, and  $e$  is the elementary charge. We assume that only nanoantenna interacts directly with the incident field which reflects the fact that exciton and trion extinction is negligible compared to that of the plasmonic nanostructure [45]. The scattering cross-section of the coupled system, being dominated by the nanoparticle dipole moment radiation, can be estimated in this phenomenological approach as  $\sigma_{scat} \propto |e\ddot{x}_{pl}|^2 \propto \omega^4 |x_{pl}|^2$ . Finally, we note that this approach can be easily generalized to an arbitrary number of coupled oscillators.

## REFERENCES

---

- [1] J. M. Raimond, M. Brune, and S. Haroche, *Rev. Mod. Phys.* **73**, 565 (2001).
- [2] G. Khitrova, H. M. Gibbs, M. Kira, S. W. Koch, and A. Scherer, *Nat Phys* **2**, 81 (2006).
- [3] S. Smolka, W. Wuester, F. Haupt, S. Faelt, W. Wegscheider, and A. Imamoglu, *Science* **346**, 332 (2014).
- [4] P. Törmä and W. L. Barnes, *Rep. Prog. Phys.* **78**, 013901 (2015).
- [5] A. E. Schlather, N. Large, A. S. Urban, P. Nordlander, and N. J. Halas, *Nano Lett.* **13**, 3281 (2013).
- [6] G. Zengin, M. Wersäll, S. Nilsson, T. J. Antosiewicz, M. Käll, and T. Shegai, *Phys. Rev. Lett.* **114**, 157401 (2015).

- [7] K. Santhosh, O. Bitton, L. Chuntonov, and G. Haran, *Nature Communications* **7**, ncomms11823 (2016).
- [8] R. Chikkaraddy, B. de Nijs, F. Benz, S. J. Barrow, O. A. Scherman, E. Rosta, A. Demetriadou, P. Fox, O. Hess, and J. J. Baumberg, *Nature* **535**, 127 (2016).
- [9] M. Wersäll, J. Cuadra, T. J. Antosiewicz, S. Balci, and T. Shegai, *Nano Lett.* **17**, 551 (2017).
- [10] K. F. Mak, C. Lee, J. Hone, J. Shan, and T. F. Heinz, *Phys. Rev. Lett.* **105**, 136805 (2010).
- [11] K. F. Mak, K. He, C. Lee, G. H. Lee, J. Hone, T. F. Heinz, and J. Shan, *Nat Mater* **12**, 207 (2013).
- [12] J. S. Ross, S. Wu, H. Yu, N. J. Ghimire, A. M. Jones, G. Aivazian, J. Yan, D. G. Mandrus, D. Xiao, W. Yao, and X. Xu, *Nat Commun* **4**, 1474 (2013).
- [13] J. S. Ross, P. Klement, A. M. Jones, N. J. Ghimire, J. Yan, D. G. Mandrus, T. Taniguchi, K. Watanabe, K. Kitamura, W. Yao, D. H. Cobden, and X. Xu, *Nat Nano* **9**, 268 (2014).
- [14] K. F. Mak, K. He, J. Shan, and T. F. Heinz, *Nat Nano* **7**, 494 (2012).
- [15] H. Zeng, J. Dai, W. Yao, D. Xiao, and X. Cui, *Nat Nano* **7**, 490 (2012).
- [16] Y. Li, A. Chernikov, X. Zhang, A. Rigosi, H. M. Hill, A. M. van der Zande, D. A. Chenet, E.-M. Shih, J. Hone, and T. F. Heinz, *Phys. Rev. B* **90**, 205422 (2014).
- [17] X. Liu, T. Galfsky, Z. Sun, F. Xia, E.-c. Lin, Y.-H. Lee, S. Kéna-Cohen, and V. M. Menon, *Nat Photon* **9**, 30 (2015).
- [18] S. Dufferwiel, S. Schwarz, F. Withers, A. a. P. Trichet, F. Li, M. Sich, O. D. Pozo-Zamudio, C. Clark, A. Nalitov, D. D. Solnyshkov, G. Malpuech, K. S. Novoselov, J. M. Smith, M. S. Skolnick, D. N. Krizhanovskii, and A. I. Tartakovskii, *Nature Communications* **6**, 8579 (2015).
- [19] M. Sidler, P. Back, O. Cotlet, A. Srivastava, T. Fink, M. Kroner, E. Demler, and A. Imamoglu, *Nat Phys* **13**, 255 (2017).
- [20] W. Liu, B. Lee, C. H. Naylor, H.-S. Ee, J. Park, A. T. C. Johnson, and R. Agarwal, *Nano Lett.* **16**, 1262 (2016).
- [21] S. Wang, S. Li, T. Chervy, A. Shalabney, S. Azzini, E. Orgiu, J. A. Hutchison, C. Genet, P. Samorì, and T. W. Ebbesen, *Nano Lett.* **16**, 4368 (2016).
- [22] J. Kern, A. Trügler, I. Niehues, J. Ewering, R. Schmidt, R. Schneider, S. Najmaei, A. George, J. Zhang, J. Lou, U. Hohenester, S. Michaelis de Vasconcellos, and R. Bratschitsch, *ACS Photonics* **2**, 1260 (2015).
- [23] S. Najmaei, A. Mlayah, A. Arbouet, C. Girard, J. Léotin, and J. Lou, *ACS Nano* **8**, 12682

- (2014).
- [24] S. Butun, S. Tongay, and K. Aydin, *Nano Lett.* **15**, 2700 (2015).
  - [25] B. Lee, J. Park, G. H. Han, H.-S. Ee, C. H. Naylor, W. Liu, A. C. Johnson, and R. Agarwal, *Nano Lett.* **15**, 3646 (2015).
  - [26] H. Chen, J. Yang, E. Rusak, J. Straubel, R. Guo, Y. W. Myint, J. Pei, M. Decker, I. Staude, C. Rockstuhl, Y. Lu, Y. S. Kivshar, and D. Neshev, *Scientific Reports* **6**, 22296 (2016).
  - [27] J. Li, Q. Ji, S. Chu, Y. Zhang, Y. Li, Q. Gong, K. Liu, and K. Shi, *Scientific Reports* **6**, 23626 (2016).
  - [28] J. Bellessa, C. Bonnand, J. C. Plenet, and J. Mugnier, *Phys. Rev. Lett.* **93**, 036404 (2004).
  - [29] D. Melnikau, R. Esteban, D. Savateeva, A. Sánchez-Iglesias, M. Grzelczak, M. K. Schmidt, L. M. Liz-Marzán, J. Aizpurua, and Y. P. Rakovich, *J. Phys. Chem. Lett.* **7**, 354 (2016).
  - [30] T. Schwartz, J. A. Hutchison, C. Genet, and T. W. Ebbesen, *Phys. Rev. Lett.* **106**, 196405 (2011).
  - [31] A.-L. Baudrion, A. Perron, A. Veltri, A. Bouhelier, P.-M. Adam, and R. Bachelot, *Nano Lett.* **13**, 282 (2013).
  - [32] P. Vasa, R. Pomraenke, G. Cirmi, E. De Re, W. Wang, S. Schwieger, D. Leipold, E. Runge, G. Cerullo, and C. Lienau, *ACS Nano* **4**, 7559 (2010).
  - [33] P. Vasa, W. Wang, R. Pomraenke, M. Lammers, M. Maiuri, C. Manzoni, G. Cerullo, and C. Lienau, *Nat Photon* **7**, 128 (2013).
  - [34] S. R. K. Rodriguez, J. Feist, M. A. Verschuuren, F. J. Garcia Vidal, and J. Gómez Rivas, *Phys. Rev. Lett.* **111**, 166802 (2013).
  - [35] A. I. Väkeväinen, R. J. Moerland, H. T. Rekola, A.-P. Eskelinen, J.-P. Martikainen, D.-H. Kim, and P. Törmä, *Nano Lett.* **14**, 1721 (2014).
  - [36] M. Ramezani, A. Halpin, A. I. Fernández-Domínguez, J. Feist, S. R.-K. Rodriguez, F. J. Garcia-Vidal, and J. G. Rivas, *Optica, OPTICA* **4**, 31 (2017).
  - [37] R. Rapaport, R. Harel, E. Cohen, A. Ron, E. Linder, and L. N. Pfeiffer, *Phys. Rev. Lett.* **84**, 1607 (2000).
  - [38] R. Rapaport, A. Qarry, E. Cohen, A. Ron, and L. Pfeiffer, *phys. stat. sol. (b)* **227**, 419 (2001).
  - [39] R. Rapaport, E. Cohen, A. Ron, E. Linder, and L. N. Pfeiffer, *Phys. Rev. B* **63**, 235310 (2001).
  - [40] M. T. Rakher, N. G. Stoltz, L. A. Coldren, P. M. Petroff, and D. Bouwmeester, *Phys. Rev.*

- Lett. **102**, 097403 (2009).
- [41] E. Orgiu, J. George, J. A. Hutchison, E. Devaux, J. F. Dayen, B. Doudin, F. Stellacci, C. Genet, J. Schachenmayer, C. Genes, G. Pupillo, P. Samorì, and T. W. Ebbesen, *Nat Mater* **14**, 1123 (2015).
- [42] B. Zhu, X. Chen, and X. Cui, *Sci. Rep.* **5** (2015), 10.1038/srep09218.
- [43] R. Jin, Y. Charles Cao, E. Hao, G. S. Métraux, G. C. Schatz, and C. A. Mirkin, *Nature* **425**, 487 (2003).
- [44] A. Arora, M. Koperski, K. Nogajewski, J. Marcus, C. Faugeras, and M. Potemski, *Nanoscale* **7**, 10421 (2015).
- [45] X. Wu, S. K. Gray, and M. Pelton, *Opt. Express*, OE **18**, 23633 (2010).
- [46] G. Zengin, G. Johansson, P. Johansson, T. J. Antosiewicz, M. Käll, and T. Shegai, *Scientific Reports* **3**, 3074 (2013).
- [47] K. P. O'Donnell and X. Chen, *Appl. Phys. Lett.* **58**, 2924 (1991).
- [48] M. Liu, M. Pelton, and P. Guyot-Sionnest, *Phys. Rev. B* **79**, 035418 (2009).
- [49] T. J. Antosiewicz, S. P. Apell, and T. Shegai, *ACS Photonics* **1**, 454 (2014).
- [50] C. Grenier, C. Ciuti, and A. Imamoglu, arXiv:1507.02480 [cond-mat, physics:quant-ph] (2015), arXiv: 1507.02480.
- [51] G. Moody, C. K. Dass, K. Hao, C.-H. Chen, L.-J. Li, A. Singh, K. Tran, G. Clark, X. Xu, G. Berghäuser, E. Malic, A. Knorr, and X. Li, *Nature Communications* **6**, 8315 (2015).
- [52] P. Dey, J. Paul, Z. Wang, C. Stevens, C. Liu, A. Romero, J. Shan, D. Hilton, and D. Karaickaj, *Phys. Rev. Lett.* **116**, 127402 (2016).
- [53] E. D. Palik, *Handbook of optical constants of solids* (Academic Press, 1998).
- [54] R. Ruppin, *Physics Letters A* **299**, 309 (2002).
- [55] A. F. Koenderink, *Opt. Lett.*, OL **35**, 4208 (2010).
- [56] C. Sauvan, J. P. Hugonin, I. S. Maksymov, and P. Lalanne, *Phys. Rev. Lett.* **110**, 237401 (2013).
- [57] P. T. Kristensen and S. Hughes, *ACS Photonics* **1**, 2 (2014).
- [58] Z.-J. Yang, T. J. Antosiewicz, and T. Shegai, *Opt. Express*, OE **24**, 20373 (2016).
- [59] E. J. Sie, J. W. McIver, Y.-H. Lee, L. Fu, J. Kong, and N. Gedik, *Nat Mater* **14**, 290 (2015).
- [60] A. M. Jones, H. Yu, N. J. Ghimire, S. Wu, G. Aivazian, J. S. Ross, B. Zhao, J. Yan, D. G. Mandrus, D. Xiao, W. Yao, and X. Xu, *Nat Nano* **8**, 634 (2013).

- [61] G. Wang, L. Bouet, D. Lagarde, M. Vidal, A. Balocchi, T. Amand, X. Marie, and B. Urbaszek, Phys. Rev. B **90**, 075413 (2014).
- [62] B. Ganchev, N. Drummond, I. Aleiner, and V. Fal'ko, Phys. Rev. Lett. **114**, 107401 (2015).
- [63] S. Mouri, Y. Miyauchi, and K. Matsuda, Nano Lett. **13**, 5944 (2013).
- [64] J. Feist and F. J. Garcia-Vidal, Phys. Rev. Lett. **114**, 196402 (2015).
- [65] J. Schachenmayer, C. Genes, E. Tignone, and G. Pupillo, Phys. Rev. Lett. **114**, 196403 (2015).
- [66] A. Castellanos-Gomez, M. Buscema, R. Molenaar, V. Singh, L. Janssen, H. S. J. van der Zant, and G. A. Steele, 2D Materials **1**, 011002 (2014)

**Supplemental Information for:**  
**Observation of tunable charged exciton polaritons in hybrid  
monolayer WS<sub>2</sub> – plasmonic nanoantenna system**

Jorge Cuadra, Denis G. Baranov, Martin Wersäll, Ruggero Verre, Tomasz J. Antosiewicz,  
and Timur Shegai

*Department of Applied Physics, Chalmers University of Technology, 412 06 Göteborg,  
Sweden*

*Centre of New Technologies, University of Warsaw, Banacha 2c, 02-097 Warszawa, Poland*

**CONTENTS**

References	16
1. Bare nanoprism data:	22
2. DF for positive and negative detuning:	23
3. Reflectivity and photoluminescence of monolayer WS <sub>2</sub> vs temperature and vs polymer adhesion layer:	24
4. Coupled system without polymer adhesion layer	26
5. Semiconductor model:	27
6. Rabi Oscillations:	28
7. Plasmon-Exciton-Trion Hamiltonian:	29
Supplementary References	31

1. Bare nanoprism data:

Figure S1 displays the DF spectra as a function of temperature for an individual bare Ag nanoprism. The decrease of the temperature from 300 K until about 225 K (Debye temperature  $T_D$  for bulk silver is  $\sim 235$  K) causes a red-shift of the plasmonic resonance. Below  $T_D$ , damping due to electron-phonon scattering is reduced and the plasmon's resonance barely moves and exhibits a saturation [1].

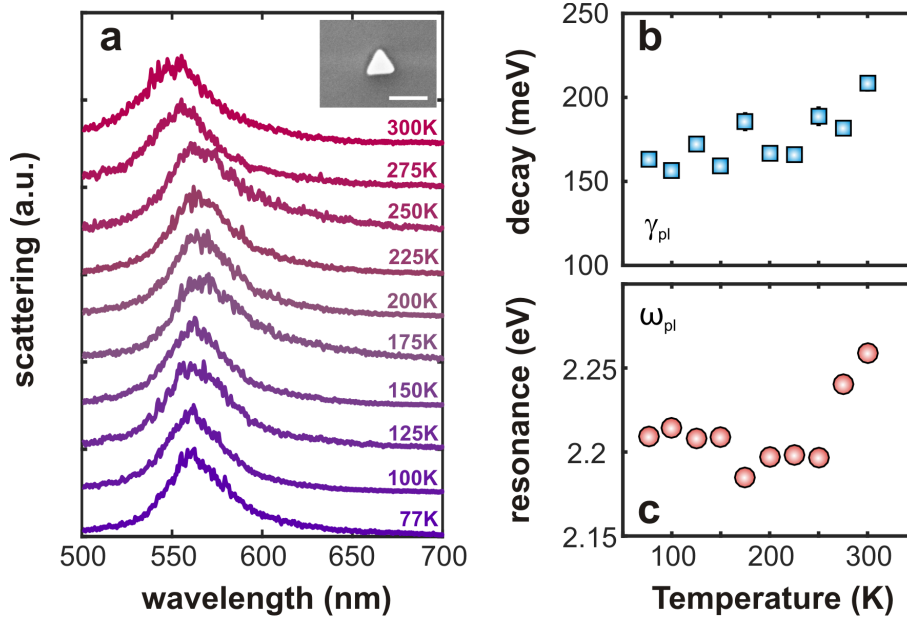


Figure S1. Temperature dependency of the uncoupled systems. a) DF spectra as a function of temperature for a silver prism on Si/SiO<sub>2</sub> substrate. The plasmonic resonance shifts its position towards low energies as the temperature is decreased. Inset corresponds to the SEM image showing the nanoprism; scale bar 50 nm. b) Temperature dependence of the PL for the same flake shown in Fig. 2. At 300 K the spectrum is dominated by the exciton whereas the trion is weaker. As the temperature is decreased both resonances blue-shift. At 77 K the trion dominates the PL spectrum.

2. *DF for positive and negative detuning:*

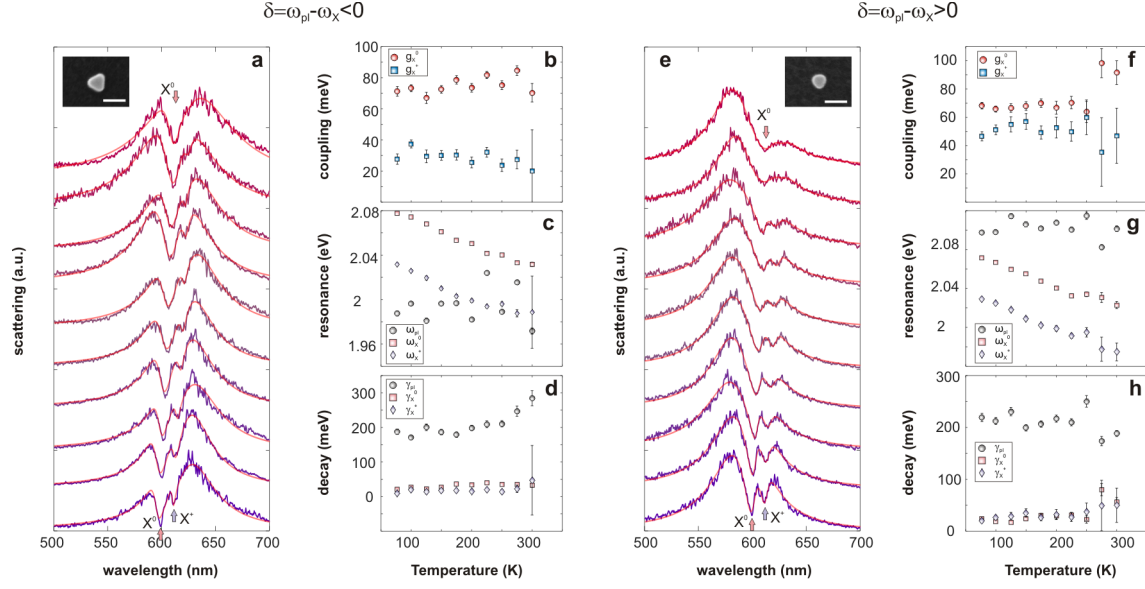


Figure S2. Temperature dependence of the coupled system for positive and negative detuning. (a-d) the case of negative detuning, (e-h) the case of positive detuning. (a, e) Dark field spectra for an individual silver nanoprism – monolayer WS<sub>2</sub> hybrid as a function of temperature. Semi-transparent red curves show coupled oscillator model fits of the data. Inset: SEM image of the corresponding nanostructure (scale bar - 100 nm). (b-d and f-h) Temperature dependence of the coupled oscillator model parameters. (b, f) coupling rates for exciton and trion, (c, g) resonance energies of plasmon, exciton and trion resonances, (d, h) decay rates for plasmon, exciton and trion correspondingly.

3. *Reflectivity and photoluminescence of monolayer WS<sub>2</sub> vs temperature and vs polymer adhesion layer:*

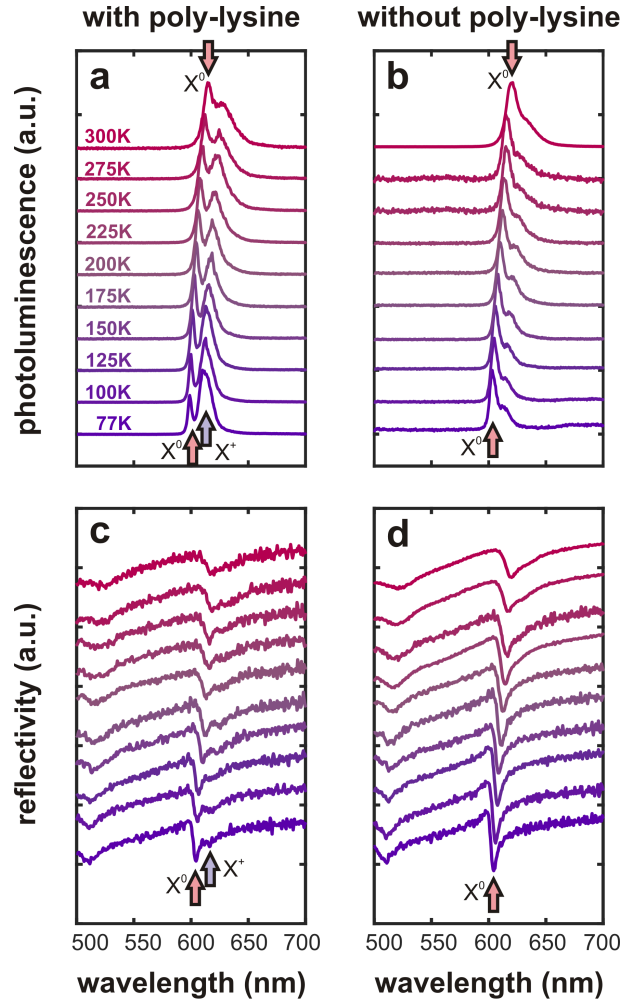


Figure S3. Reflectivity measurements. (a) PL spectra for  $T = 77 - 300$  K when the polymer adhesion layer was used. At low temperature both exciton and trion resonances are well resolved. As the temperature is raised the trion is less visible. (b) Same as in (a) but without the polymer adhesion layer. The trion resonance is not observed for any temperature, whereas the exciton is observed for all temperatures as in a). (c) Reflectivity spectra for  $T = 77 - 300$  K when the polymer adhesion layer is used. A- and B-excitons are seen for all temperatures. For the A-exciton at low temperature both exciton and trion resonances are resolved, as the temperature is raised the trion is less visible. (d) Same as in (c) but without the polymer adhesion layer. The trion resonance is not observed in reflectivity measurements for any temperature, whereas the exciton is observed for all temperatures as in c).

Role of the polymer adhesion layer: The polymer adhesion layer not only ensures a proper density of nanoprisms but also changes the excitonic specimens (Fig. S3). For samples with adhesion layer the PL at low temperature is dominated by the trion whereas in samples without adhesion layer the exciton prevails in the PL spectra. This is caused by a chemical doping of p-type carriers (positively charged poly-lysine molecules) and stabilization of a positively charged trion state in the system [2].

4. *Coupled system without polymer adhesion layer*

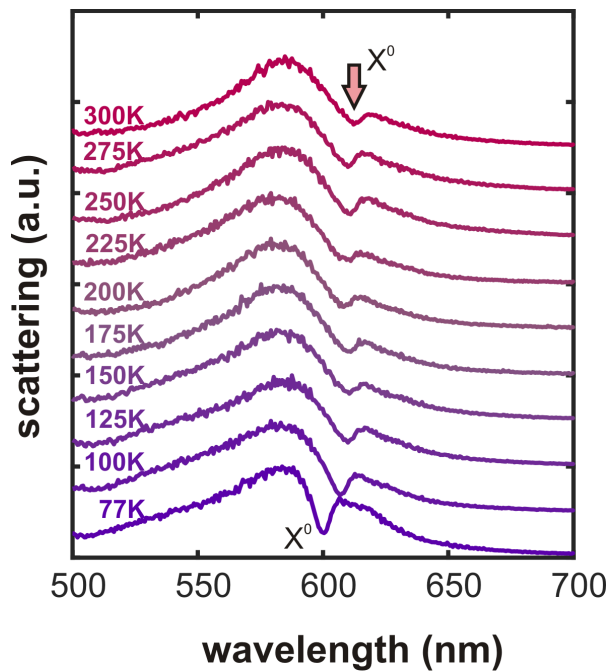


Figure S4. Samples without polymer adhesion layer. (a) Dark field spectra as a function of the temperature shows the interaction with the neutral exciton state. (b) PL spectra for the uncoupled monolayer without adhesion layer. Inset in a) depicts the SEM of the prism on top of the monolayer; scale bar 50 nm. The insets illustrates the optical micrograph and dark field images of the monolayer; scale bar 25  $\mu\text{m}$ .

5. *Semiconductor model:*

The O'Donnel model gives the following values of  $E_g(0) = 2.07$  eV (2.02 eV),  $S = 1.78$  (2.0) and  $\langle \hbar\omega \rangle = 25$  meV (33 meV) for  $X^0$  ( $X^+$ ) correspondingly. The different values of  $\langle \hbar\omega \rangle$  for  $X^0$  and  $X^+$  might come from the fact that our temperature range covers only the decaying part of T (for T below 77 K the peak position reaches a quasi-steady state and both resonances barely move). The extracted parameters agree with previously reported values [3]. It is worth noticing that the  $\langle \hbar\omega \rangle$ , although different for exciton and trion, is similar to the energy of the LA phonon [4]. The  $S$  value is rather homogeneous among TMD monolayer and increases as the number of layers is decreased [5] this implies a strong electron-phonon coupling caused by confinement owned by the monolayer.

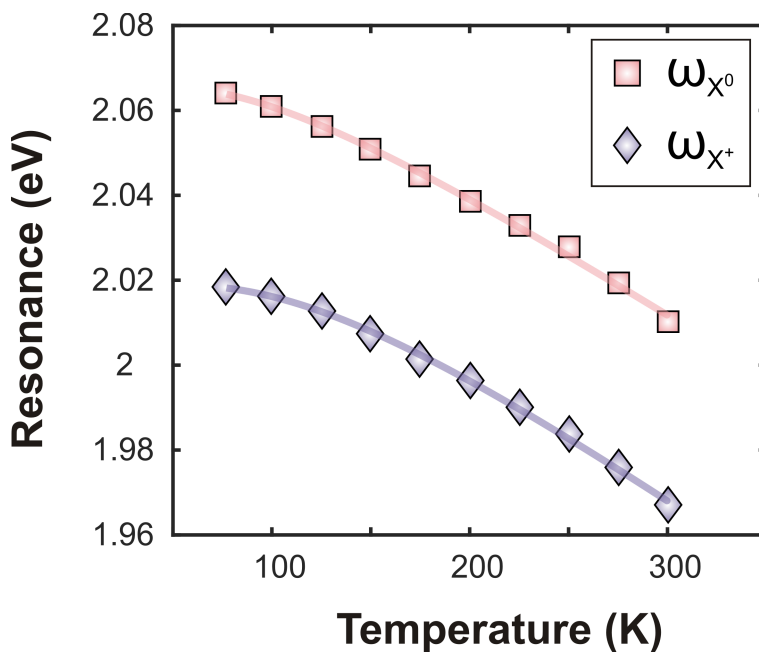


Figure S5. Uncoupled exciton and trion vs temperature. Uncoupled exciton and trion resonances extracted from the PL data in Fig. S3a. O'Donnel fits are shown by solid lines. The O'Donnel model gives the following values of  $E_g(0) = 2.07$  eV (2.02 eV),  $S = 1.78$  (2.0) and  $\langle \hbar\omega \rangle = 25$  meV (33 meV) for  $X^0$  ( $X^+$ ) correspondingly.

6. *Rabi Oscillations:*

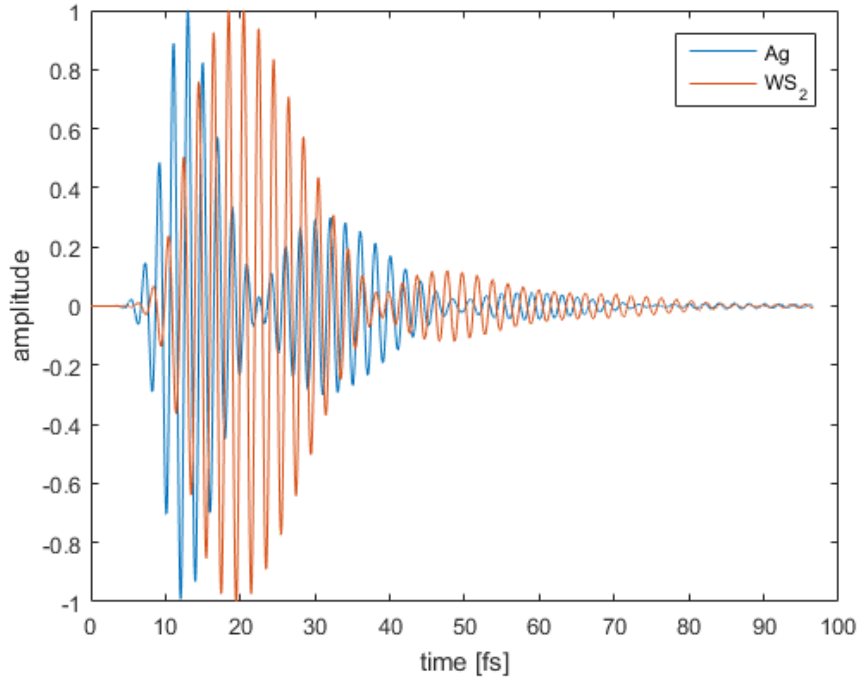


Figure S6. Visualisation of Rabi oscillations using FDTD. Field amplitudes as a function of time. Note ultrafast energy transfer between metal and WS<sub>2</sub> corresponding to several Rabi cycles. To monitor the temporal evolution of the excited we track the amplitude of the electric field of the plasmon of the Ag nanoprism and the auxiliary electric field in the WS<sub>2</sub>, which is a measure of the amount of energy stored in the 2D material in the form of excitons.

7. *Plasmon-Exciton-Trion Hamiltonian:*

To understand the dynamics of the coupled system we analyze the eigen problem of the Hamiltonian describing the coupled system. We use the following basis:  $|1, g, g\rangle$ ,  $|0, e, g\rangle$ ,  $|0, g, e\rangle$ , where the corresponding symbols refer to plasmon, exciton and trion excitations. These notations lead to the following Hamiltonian:

$$\frac{\hat{H}}{\hbar} = \begin{pmatrix} \omega_{pl} - i\gamma_{pl} & g_{X^0} & g_{X^+} \\ g_{X^0} & \omega_{X^0} - i\gamma_{X^0} & 0 \\ g_{X^+} & 0 & \omega_{X^+} - i\gamma_{X^+} \end{pmatrix}$$

Here  $\omega_{pl}$ ,  $\omega_{X^0}$ ,  $\omega_{X^+}$  and  $\gamma_{pl}$ ,  $\gamma_{X^0}$ ,  $\gamma_{X^+}$  are resonance frequencies and dissipation rates for plasmon, exciton and trion respectively. The coupling strength between plasmon-exciton and plasmon-trion are denoted as  $g_{X^0}$  and  $g_{X^+}$  correspondingly. Possible exciton-exciton, trion-trion and exciton-trion interactions are neglected in this model.

There are three hybrid states (lower – LP, middle – MP and upper – UP polaritons) arising from solving the eigenvalues of the system. These hybrid states may be expressed as linear combinations of the original plasmon, exciton and trion excitations with complex valued coefficients. The absolute square values of the coefficients give insight on the plasmonic, excitonic and trionic contributions to each polariton branch.

We solve the corresponding eigen problem numerically. The contributions from each constituent system to the polariton branches turn out to be highly dependent on the coupling strength and the detuning. By studying the results when combined strong coupling ( $2\sqrt{g_{X^0}^2 + g_{X^+}^2} \gtrsim \gamma_{pl}$ ) is just reached the MP contains a photonic component close to  $\sim 20\%$  (see Fig. S7a). Though in the very strong coupling case ( $2g_{X^0} > \gamma_{pl}, \gamma_{X^0}$ ) where the coupling also exceeds the detuning between exciton and trion states, the plasmonic component nearly disappears and thus the middle polariton becomes dark (see Fig. S7b). Since this is not observed in the experiment (see Main text), we conclude that our system adopts the just reached combined strong coupling regime in agreement with Fig. S7a.

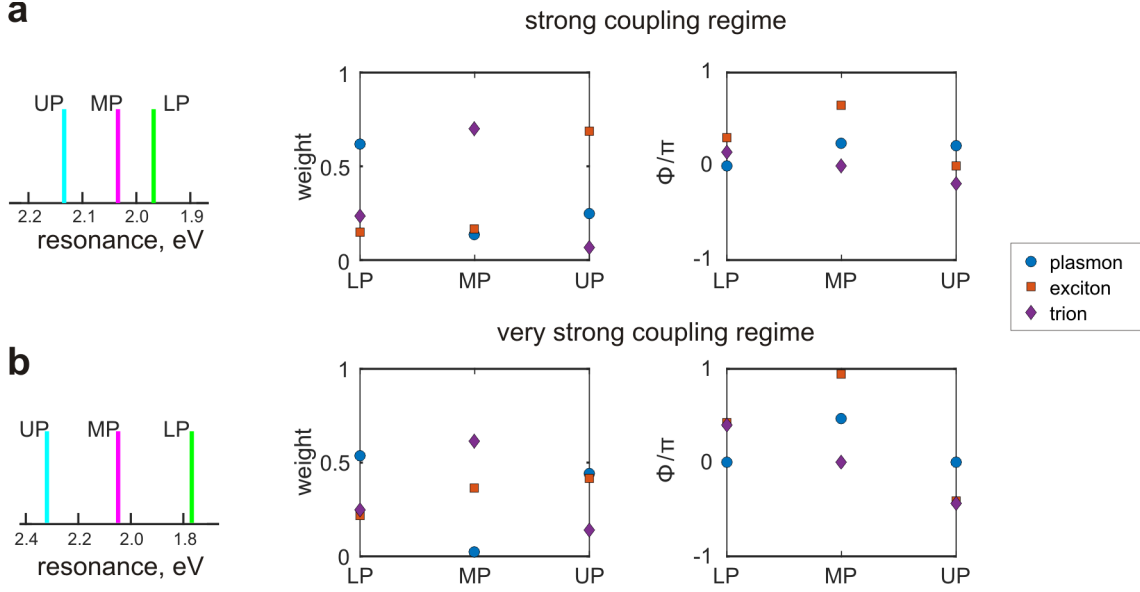


Figure S7. Intermediate and strong coupling regimes in  $3 \times 3$  Hamiltonian. (a) Intermediate coupling regime is modelled by setting the following parameter values:  $\omega_{pl} = 2.02$  eV,  $\omega_{X^0} = 2.10$  eV,  $\omega_{X^+} = 2.01$  eV;  $\gamma_{pl} = 200$  meV,  $\gamma_{X^0} = 50$  meV,  $\gamma_{X^+} = 60$  meV;  $g_{X^0} = 80$  meV,  $g_{X^+} = 64$  meV. These values are extracted from the experimental data using the coupled oscillator model. Note that MP has approximately 20% plasmon contribution meaning that MP is bright. (b) Strong coupling regime is modelled by setting the following parameter values:  $\omega_{pl} = 2.02$  eV,  $\omega_{X^0} = 2.10$  eV,  $\omega_{X^+} = 2.01$  eV;  $\gamma_{pl} = 200$  meV,  $\gamma_{X^0} = 50$  meV,  $\gamma_{X^+} = 60$  meV;  $g_{X^0} = 220$  meV,  $g_{X^+} = 176$  meV. Note that MP has nearly zero plasmon contribution meaning that MP is essentially dark.

- 
- [1] M. Liu, M. Pelton, and P. Guyot-Sionnest, *Phys. Rev. B* **79**, 035418 (2009).
- [2] S. Mouri, Y. Miyauchi, and K. Matsuda, *Nano Lett.* **13**, 5944 (2013).
- [3] A. T. Hanbicki, M. Currie, G. Kioseoglou, A. L. Friedman, and B. T. Jonker, *Solid State Communications* **203**, 16 (2015).
- [4] Z. Jin, X. Li, J. T. Mullen, and K. W. Kim, *Phys. Rev. B* **90**, 045422 (2014).
- [5] A. Arora, M. Koperski, K. Nogajewski, J. Marcus, C. Faugeras, and M. Potemski, *Nanoscale* **7**, 10421 (2015)